Mathematical Modelling of the Morphology of Streptomyces Species

Rudibert King

Institut für Prozeß- und Anlagentechnik, Fachgebiet Meß- und Regelungstechnik, Technische Universität Berlin, Budapester Str. 48, 10787 Berlin, Germany
E-mail: king0630@mailszrz.zrz.tu-berlin.de

List of Symbols and Abbreviations

a_i	coefficient of the lumped pellet model
A	area
c_i	concentration of substance i

Advances in Biochemical Engineering/ Biotechnology, Vol. 60
Managing Editor: Th. Scheper

c_{Hy}	hyphal concentration
c_{Tip}	concentration of tips
D	diffusion coefficient
f	number density function
F	total number of particles per volume
g	concentration based on cell's volume
HGU	hyphal growth unit
k	rate constant
l_i	coordinate of i-th section, i = 1, 2, 3
l_0	length of a hypha associated with one nucleotide, or length of a spore
L_i	length of i-th section
M	number of substrates
N	number of tips
p	density of the breaking probability
q	specific volumetric flow
Q	volumetric flow
r	reaction rate
$r_{Hy,Tip}$	synthesis rate of hyphae, tips
$r_{HyD,TipD}$	degradation rate of hyphae, tips
$r_{HyB,TipB}$	breakage rate of hyphae, tips
s	characteristic property
t	time
u	growth rate along a characteristic property
V	volume
Y	yield coefficient
z	spatial coordinate
z_R	radius of a pellet

Greek symbols

α	apical growth velocity
β	branching rate
γ	constant
λ	constant
μ	specifc rate
σ	source or sink
ψ_{Hy}	activity of branching
ψ_{Tip}	activity of apical growth

1 Introduction

About 70% of all antibiotics known today are produced by *Actinomycetales*, about 90% of which are related to *Streptomyces* species [1]. Other metabolites such as vitamin B12 and industrial enzymes, e.g. glucose isomerase, are also produced by streptomycetes [1].

Despite their industrial importance, knowledge about the primary metabolism [2, 3] and morphology of streptomycetes is rather limited. In recent decades much effort has focussed on the discovery of new antibiotics and on the improvement of the respective production methods. However, when problems of up-scaling of a cultivation on a rational basis, or design of modern model-based concepts of control engineering, are addressed, more information about the fundamental growth behaviour is needed with respect to morphology, primary and secondary metabolism.

In this contribution the main emphasis will be put on a morphological description of *Streptomyces* cultures. The models developed can be used for a better interpretation of basic phenomena observed in such processes. It will be shown in the following that morphological models:

(a) provide a tool to better understand the complex fundamental growth behaviour, which is especially important when correlations between morphology and productivity are proposed [4];
(b) provide a means to test biochemical hypotheses in a dynamic context;
(c) form a basis on which more complex models including a detailed description of metabolism [5, 6] can be build up in the future; and
(d) can be used to solve dedicated technical problems.

The modelling of the morphology of *Streptomyces* species will be done from different points of view (see Fig. 1). In the first part a microscopic approach is chosen to address more fundamental questions of morphology. The second part is devoted to a macroscopic description of single pellets which reveals the influences of mass transport on growth and production. In the last part the behaviour of a cultivation with pellets of different sizes is explained. Although the models have been developed for *Streptomyces* species in the first place, a major part of the models can also be used for fungal cultivations.

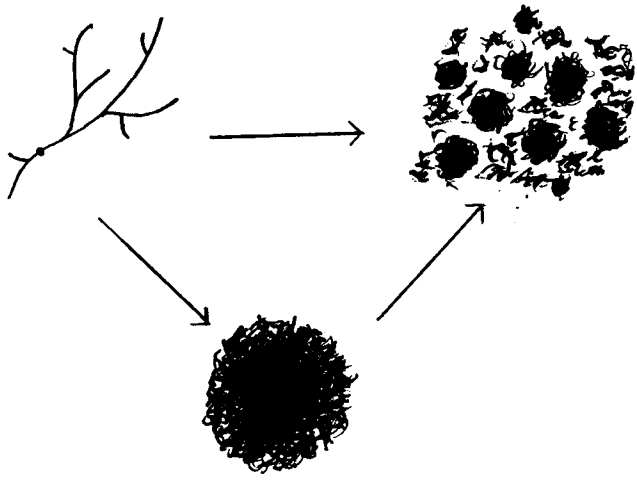

Fig. 1. Different aspects of morphology

2
Microscopic Morphology

Biological details about the processes leading to hyphal elongation and branching in streptomycetes are only known to a very limited extent. A summary of the available information shows that for the development of a dynamic model many questions have even not been stated. In many biologically orientated publications it is evident, however, that elongation and branching cannot be explained satisfactorily if a consideration of dynamic processes is omitted. Hence, only mathematical models can help.

Up to now only a few attempts to describe microscopic growth have been made even when models for fungi are included in this review. A large group of models considers lumped parameters only, such as the number of tips, the total length of all hyphae or producing and non-producing hyphae [7–14]. These models do not give a correct geometric picture of the mycelium and do not contribute to a better understanding of the complex morphological growth patterns. More sophisticated approaches have to be adopted. Apart from some models proposed for fungi [15–17] mainly one research group is active in this area [18–21].

A detailed description of morphology is interesting, for example if a correlation between morphology and productivity is found. Unfortunately, only very few data are available in this respect [4, 10, 22, 23]. However, a quantitative experimental determination of morphology and therefore a systematic approach to solve this problem became possible only a few years ago with modern image analysis systems, see Paul and Thomas in this volume, or [24].

2.1
A model of Microscopic Growth

As a first step, hyphal elongation will be considered. Branching will then be formulated as a process depending on DNA-duplication.

2.1.1
Hyphal Elongation

Experimental investigations indicate that a constant maximum elongation velocity is preceded by an acceleration phase; see for example [25]. Radioactive labelling techniques reveal a purely apical growth with no incorporation of precursors in subapical regions [25]. From the increasing elongation velocity it is concluded that precursors for cell wall synthesis are not only produced at the tip but in a growing compartment behind the tip. This compartment is separated from subapical regions by septa. Prosser and Tough [25] assume a diffusive transport of the precursors to the tip since a cytoskeleton is not known in streptomyces strains. In the following considerations production, transport and incorporation of precursors is assumed to be the rate limiting step in hyphal elongation. To derive a model, a schematic part of a mycelium is sketched in Fig. 2. It consists of a mother compartment (2, 3) of constant length

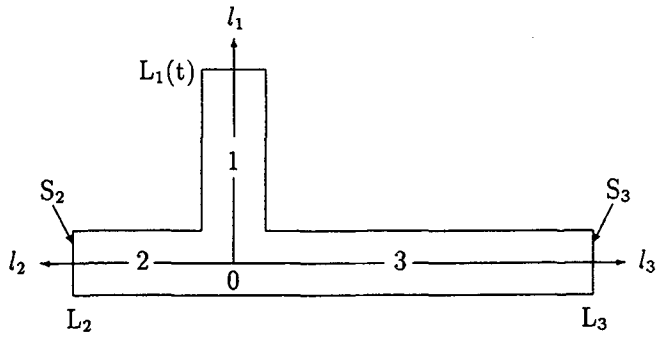

Fig. 2. Schematic representation of a section of a mycelium. S_i – septum at the border of the i-th section of a mother compartment

which is bounded by two inpermeable septa (S_2, S_3) and an apically growing hypha (1).

The model formulation follows the lines shown in [19, 20]. It is assumed that a limiting precursor P is produced in all parts (1, 2, 3) with a velocity $r_P(t, L_i)$. The precursor is degraded by a reaction which is assumed to be first order ($k_d \cdot g_P$) for simplicity. P is transported to the tip by diffusion only. For a constant cross-sectional area A of a hypha a balance yields

$$\frac{\partial g_P(t, l_i)}{\partial t} = D_P \frac{\partial^2 g_P(t, l_i)}{\partial l_i^2} + r_P(t, l_i) - k_d \cdot g_P(t, l_i), \quad i = 1, 2, 3$$

$$t > 0, \quad l_i \in (0, L_i), \quad L_1 = L_1(t) \tag{1}$$

where l_1, l_2 and l_3 are the co-ordinates of the three parts of the mycelium shown in Fig. 2.

In general, the synthesis velocity $r_P(t, l_i)$ is a function of the physiological state of a hypha at $l_i = \xi$, and a function of the local extracellular medium composition. For small mycelia external gradients can be neglected. Therefore, a homogeneous medium composition is assumed. Although a first approach to describe the effects of a time-variant medium composition can be found in [17, 26, 27] a constant composition is assumed here additionally for simplicity.

Little information is available on the spatial distribution of the physiological state in a hypha. It was found for example [28, 29] that DNA- and RNA-synthesis did not show a profound distribution along a hypha. Protein biosynthesis, in contrast, was not constant when mycelia were broken down in 10 μm sections [30]. However, in these investigations it was not known which sections were obtained from apical or subapical regions. Therefore, a constant synthesis velocity $r_P(t, l_i) = r_P$ is assumed in the following model. This assumption is supported by experiments with *S. tendae* in which branching was influenced by glucose [24] or ammonium [4, 31] but not apical elongation.

A quasi-steady state assumption of Eq. (1) is valid if synthesis, transport and consumption of P are fast compared to apical growth:

$$0 = D_P \frac{d^2 g_P(t, l_i)}{dl_i^2} + r_P - k_d \cdot g_P(t, l_i), \quad i = 1, 2, 3,$$
$$l_i \in (0, L_i), \quad L_1 = L_1(t). \tag{2}$$

This linear equation can be solved by taking into account appropriate boundary conditions, i.e. (1) septa S_2 and S_3 in Fig. 2 are impermeable [32], (2) the sum of all material flows into the origin has to disappear, and (3) it is assumed that the the flow of precursor into the tip is proportional to an increase in hyphal volume. The apical growth velocity is then given by [33]

$$\frac{dL_1(t)}{dt} = \alpha_m \cdot \frac{e^{2\omega L_1(t)} - \delta}{e^{2\omega L_1(t)} + \delta}, \tag{3}$$

with

$$\omega = \frac{\mu_{Hy}}{\alpha_m}, \quad \delta = \frac{3 + e^{2\cdot\omega\cdot L_2} + e^{2\cdot\omega\cdot L_3} - e^{2\cdot\omega\cdot L_2}\cdot e^{2\cdot\omega\cdot L_3}}{-1 + e^{2\cdot\omega\cdot L_2} + e^{2\cdot\omega\cdot L_3} + 3\cdot e^{2\cdot\omega\cdot L_2}\cdot e^{2\cdot\omega\cdot L_3}}, \tag{4}$$

in which $\mu_{Hy} = \text{const} \cdot r_P$ is the exponential growth rate seen at the beginning of an experiment and $\alpha_m = \text{const} \cdot \sqrt{D_P/k_d} \cdot r_P$ is the constant apical growth velocity found for large $L_1(t)$. Obviously, the exponential growth rate μ_{Hy} is determined by the synthesis rate of the precursors. The maximal growth velocity α_m, however, is also a function of the ratio of degradation to diffusive transport. If degradation increases compared to transport, α_m is slowed down.

Very importantly, the only model parameters μ_{Hy} and α_m of Eqs. (3, 4) can be determined very easily in experiments. Most investigations in this respect have been performed on solid agars, although technical processes are run under submersed conditions. An exception can be found in the work of Reichl et al. [24, 34, 35]. Here growth is monitored and many parameters are determined by image analysis in a growth chamber which is continuously supplied by fresh medium. By analyzing a very large number of growing mycelia as a function of medium composition, statistically reliable data are obtained.

A first comparison between measured data [34] and a numerical integration of Eq. (3) is given in Fig. 3. It can be seen that the observed growth behaviour of a germ tube of *S. tendae* can be described very well. The growth rate, Eq. (3), derived here from a mechanistic point of view, differs significantly from the assumed growth rate for fungi; see Eq. (16) of the contribution of Krabben and Nielsen in this volume.

More examples, including fungi with impermeable septa, are given in [19, 20], where mycelial compartments with two growing tips are also described.

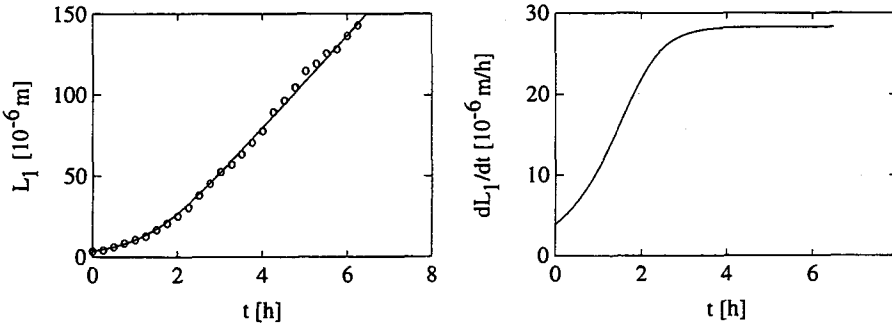

Fig. 3. Comparison of simulated (–) and measured (o) development of a germ tube of *S. tendae* with $\mu_{Hy} = 1.081/h$, $\alpha_m = 28.3$ µm/h, $L_1(0) = L_2(0) = 0$, $L_3(0) = 3.6$ µm and calculated growth velocity $dL_1(t)/dt$. The measurements are taken from [34]

2.1.2 *Branching*

When a mycelium grows the total length of all hyphae increases exponentially. This can only be explained by an exponentially increasing number of tips due to branching since individual hypha reach a maximum growth velocity. Therefore, a branching rate has to be described. To yield a geometrical picture of a mycelium which is similar to microscopic observations the branching points have to be determined, too. They seem to be related to the sites where septa are built [29, 32]. However, the sequence of septation and branching has not be revealed up to now, because stains which make septa visible without disturbing growth are not known [29, 32].

Unicellular organisms are considered first, to develop a model assumption for the septation and branching processes of mycelial organisms. A unicellular organism grows by increasing all of the cell's constituents, partitioning of the chromosomes, and then dividing the whole cell into two daughter cells. The time course of division is mainly determined by the doubling of the DNA. It is obvious [36] that the division of a unicellular organism resembles the process of septation in hyphae. Therefore, it is assumed in the following that septation is coupled to DNA-duplication and that there exists a correlation between DNA-doubling and the time and site of branching. A similar idea has been proposed already for fungi [37]. A sequence of septation and branching makes sense, since it allows the subapical part further growth using its still existing metabolic activity for synthesis all of the cell's constituents. Otherwise, the metabolism would have to be cut down drastically to nongrowth conditions. The sequence, however, assumes that branching only takes place in subapical regions. This was found in most experimental observations [32]. However, in some cases the opposite was true.

From this discussion it is clear that a mathematical description of branching has to include DNA-replication, DNA-segregation, septation and initiation of a new tip.

2.1.2.1
DNA-Replication and DNA-Segregation

In prokaryotic cells DNA is not organized in a compartment like a nucleus. After staining experiments the DNA is visible in so-called nucleotides. However, Gray et al. [38] discuss the possibility of artefacts through staining, as with the electron microscope a fibrillar structure is found instead. Therefore, it is not known exactly where DNA replicates and whether a chromosome is fixed at the tip. A duplication of the nucleotides in subapical regions is, however, proven [28]. Even in rather old subapical parts, DNA synthesis is found. From the intensity and size of the stained nucleotides it can be concluded that a segregation does not take place when a certain nucleotide concentration is exceeded. In an apically growing hypha a gradient of nucleotide concentration towards the tip is found. Mechanisms of segregation are not known as the replicon model [39], which is under discussion anyway, cannot be used for apical growth.

It can be summarized that, due to the lack of exact knowledge in the field of DNA-replication and DNA-segregation, only hypotheses can be formulated. Here mathematical modelling provides a powerful tool to compare the outcome of simulations based on such hypotheses with available measurements. An example is given in Fig. 4 in which the nucleotide pattern of a growing apical hypha is calculated based on different hypotheses [33]. The hypothesis H1 b) resembles the asymmetrical picture obtained in staining experiments. It is obtained by a very simple mathematical model [19]. The replication rate decreases according to

$$\mu_D(t,l) = k_D \cdot (g_{Dm} - g_D(t,l)), \quad g_{Dm} = \text{const.}, \tag{5}$$

where g_{Dm} represents a maximum DNA-concentration. With this expression the effect of a regulation mechanism is taken into account. DNA-replication is stopped when segregation fails, i.e. when the DNA-concentration exceeds a certain limit, g_{Dm}. A segregation to a l_0-neighbourhood takes place whenever no other nucleotides are present in this neighbourhood. The considered unit length l_0 can be defined for example as the length or section which is associated to one nucleotide.

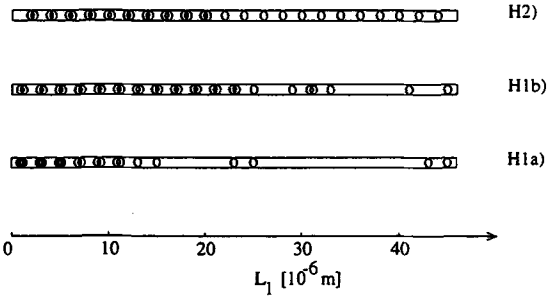

Fig. 4. Nucleotide density in a growing hypha based on different hypotheses. Number of nucleotides: ○ – one; ○○ – two, not segregated; ●● – four, not segregated

2.1.2.2
Septation

Staining experiments show that the first septum behind a tip is usually nearer to the second septum than to the tip. A ratio of 1/3 to 2/3 is often found. In subapical hyphae septa are placed in a middle position between two existing septa. As the staining experiments do not reveal when a septum was formed, different possible hypotheses could be discussed. In the following a simple model assumption will be used instead. When the number of nucleotides between two septa or between a first septum and the respective tip is doubled (e.g. $4 \rightarrow 8$) a new septum will be formed. The site of the septation is chosen in a way that on both sides the same number of nucleotides is found. With this model assumption and the saturation kinetics of Eq. (5), the above-mentioned asymmetrical and symmetrical septum distributions in apical and subapical regions are obtained, respectively. Hence, the timing and location of septation is known.

A similar approach was chosen from Prosser and Trinci [16] in a completely discretized model for the growth of fungi. For the numerical simulation of the model proposed here, Yang [19] introduces a hyphal discretization with the already mentioned unit length l_0. In the simulation, nucleotides are modelled as discrete elements. For every unit length the processes of replication and segregation have to be considered.

2.1.2.3
Branching

All processes considered up to now are described in a deterministic way. From experiments it is known, however, that the appearance of mycelia shows stochastic influences. To include these effects in a first approach, branching is modelled as a normally distributed random process. The actual sites of branch initiation and the time delay between septation and branch initiation are represented by random variables. For the first stochastic process experimental data for the mean and the variance are available with the method shown in [32]. For the latter moments have to be chosen in the simulation.

2.1.2.4
Growth and Branching Directions

To obtain a geometrical picture of hyphal growth it has to be considered that hyphae do not grow and branch in a fixed direction. Statistical investigations [21] show a normal distribution of both directions with different moments, respectively. Hence, for a simulation of the development of the unit length sections (l_0) the growth and branching directions are modelled as random processes.

2.2
Simulation and Comparison with Experimental Results

Figure 5 shows a simulation of the growth of a mycelium starting from a spore. A comparison of this 2-dimensional projection of a 3-dimensional simulation

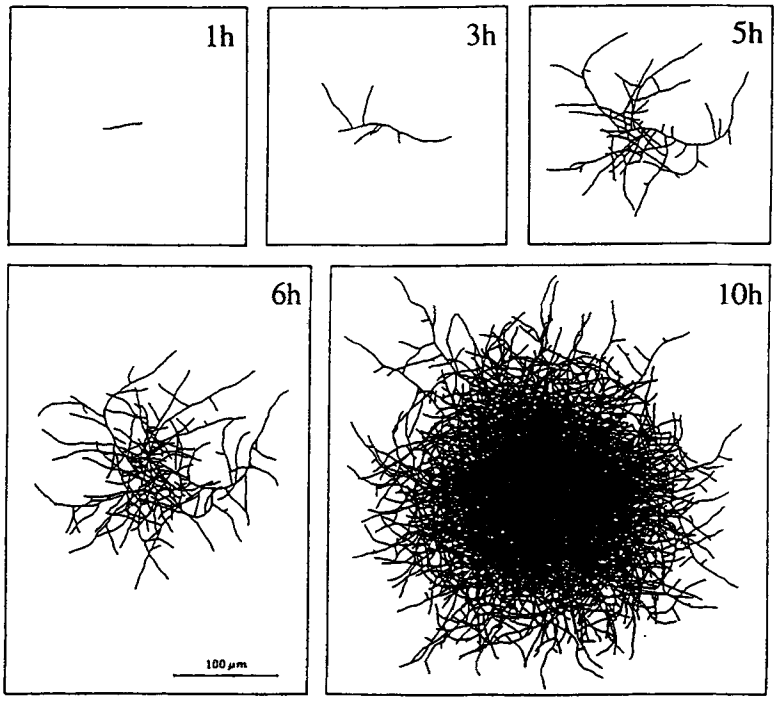

Fig. 5. A 2-dimensional projection of a 3-dimensional simulation of the growth of *S. tendae* for different time instants; from Yang et al. [20]

with real microscopic data shows a very good visual representation of the morphology. This is even enhanced when the real microscopic picture is digitized by means of an image analysis system and the thicknesses of all hyphae are then reduced to one pixel (skeletonized; see contribution of Paul and Thomas in this volume).

The quality of the simulation also becomes obvious in Fig. 6 where the measured total length of all hyphae, L_t, the number of tips, N, and the calculated 'hyphal growth unit', L_t/N, are compared to simulation results. While the evaluation with the image analysis system has to stop after about 6.25 h because of multiple crossings of hyphae and hyphae growing out of focus, the simulation can be continued until a pellet is formed. The simulation should then be stopped, too, since the assumption of a homogeneous medium supply is violated. This problem will be addressed in the next section.

Yang [26] showed with a rather ad-hoc model extension that in principle it is possible to include the influences of mechanical stress due to a stirrer as well. The breakage probability of a single hypha is modelled as a function of the history of this hypha. Microkinetic data in this respect are very rare, of course. The simulation shown in Fig. 7 displays the well known microscopic picture from samples out of a fermenter. Some more examples for the application of this model can be found in [19, 20, 26].

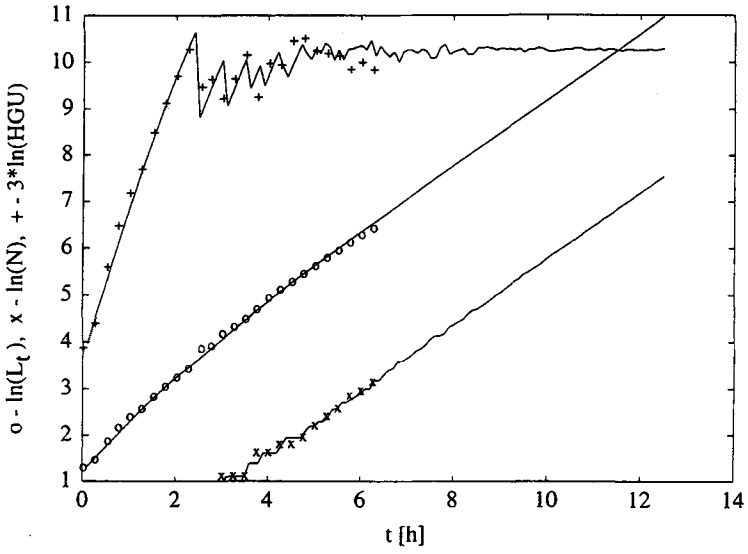

Fig. 6. Simulated and measured total hyphal length L_t (○), number of tips N (×) and hyphal growth unit HGU (+) of a mycelium of *S. tendae* from Yang et al. [20]. *Solid lines* indicate simulations

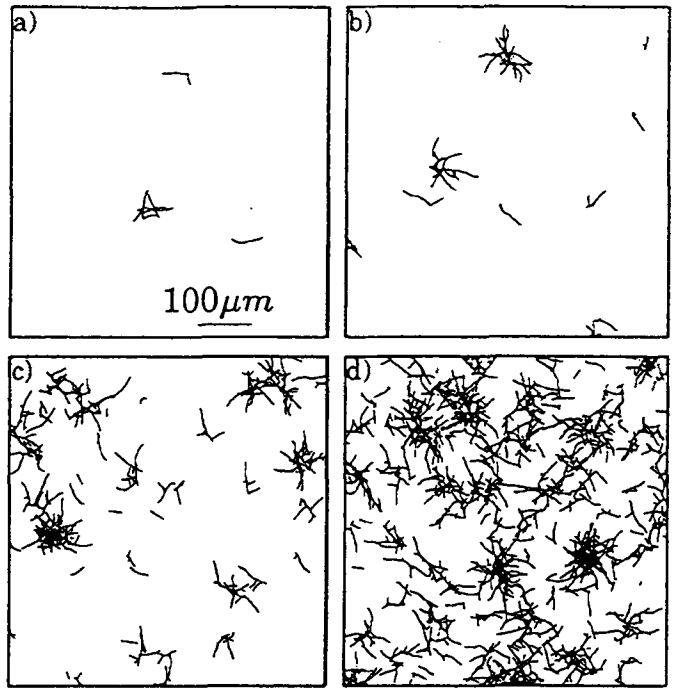

Fig. 7a–d. Growth in a fermenter: **a** t = 10 h; **b** t = 15 h; **c** t = 20 h; **d** t = 25 h; from Yang [26]

Based on this model a realistic picture of the microscopic elongation and branching behaviour is given. Simulation studies can now be used on one side to better understand the complex morphological growth patterns and to determine parameters which cannot be measured. On the other side, a number of questions can be studied. With the above-mentioned growth chamber and the image analysis system it is, for example, possible to study the influence of the medium composition on apical elongation and branching rate. Therefore, this model can be used to search systematically for (time variable) process conditions for which a specific morphology is obtained. A most interesting question will then be whether productivity has changed. This idea is based on observations with *S. tendae* in which a correlation between productivity and morphology has been found [4].

Another interesting subject deals with the genetic stability of plasmids in mycelial organisms which is known to be very critical. An experimental microscopic investigation of the segregation mechanisms without a disturbance of growth is almost impossible. A model could be used here, however, to test the macroscopic outcome of microscopic hypotheses, and to exclude at least unlikely hypotheses.

3 Morphology of a Single Pellet

Whether a cultivation should be run in such a way that there are many pellets cannot be answered from a general point of view. It is not even clear by which factors the amount, size, form and internal structure of pellets can be influenced by the operator. However, higher amounts of some interesting metabolites are produced by pellets but not by loose mycelia, although the reason for this is not understood up to now [40]. From the point of view of viscosity, and therefore mass and heat transport in the abiotic phase, pellet growth should be favoured, too. On the other hand, pellet growth is associated with a severe problem: the macroscopic structure of a pellet leads to inhomogeneities in the biophase. From measurements [41, 42] it is known, for example, that the oxygen penetration depth is somewhere near 150 μm. As a result, large pellets behave in a different way compared to small ones, and a measurement of total biomass does not bear much significance in it. Moreover, the growth and production behaviour of a single pellet is not only a function of time but a function of the location inside the pellet as well.

These problems indicate that in pellet containing cultivations phenomena and questions might appear which are unknown in cultivations with unicellular organisms. It is therefore of great interest to shed some more light onto the behaviour of growing pellets, which requires the mathematical model to be extended by the processes of mass transport into and out of a pellet. This is done in the rest of this contribution in two steps. First, a single pellet is considered. As the mathematical complexity of the proposed model is rather high a model reduction is suggested. Based on the reduced model a population balance is formulated in the second step, which describes the behaviour of a cultivation consisting of pellets of different sizes. The emphasis will again be put on

morphological details. Although the influence of the complex metabolism on growth behaviour is only taken into account by a simple, unstructured approach, basic problems of such cultivations can be discussed.

3.1 A Model of Pellet Growth

As in the case of microscopic growth, only very few approaches are known to model pellet growth. Apart from some very simple formulae to describe growth as a function of time [43–45], most of the work was done to predict the oxygen distribution in pellets with a constant radius and constant density [46–50]. Similar approaches are found in models for biofilms [51, 52]. However, the simulations shown in the last section as well as histograms [41] reveal that the biomass density in a pellet is not at all constant. A space dependent biomass density is considered only by some authors [17, 19, 27, 41, 42, 53, 54]. Wittler et al. [41] do not include growth in their model, and the profiles of biomass density are somewhat arbitrary and do not reflect the above-mentioned results. As the microscopic model introduced above is already very complex, another approach is chosen here according to Buschulte et al. [42, 53, 54], describing growth and production from a more macroscopic point of view. The model starts from the observation that pellets are usually very dense. Therefore, a description with continuous variables, such as the local concentrations of hyphae and tips, seems meaningful. As in the model for microscopic growth, the macroscopic approach also includes apical elongation and subapical branching as the main growth related processes.

3.1.1 *Hyphal Elongation*

As new branches are usually formed from rather long mother compartments ($L_2 + L_3$) an almost constant apical growth velocity follows from Eq. (3). Moreover, Yang [19] showed that in existing hyphae dL_1/dt does not change significantly, irrespective of the formation of new septa in subapical regions. The reason is the still rather long apical part of the hypha in which the supply of precursors at the tip is limited by the diffusive transport to the tip but not by the volume for production behind the tip. Therefore, an apical elongation velocity is considered which only depends on the extracellular composition of the medium, $\underline{c}_S = (c_{S1}, \ldots, c_{SM})$, but not on the microscopic morphology. From a macroscopic point of view the local elongation velocity r_{Hy} of all hyphae is therefore proportional to the local concentration of tips, c_{Tip}:

$$r_{Hy}(t, \underline{z}) = \bar{\alpha} \cdot \psi_{Tip}(\underline{c}_S(t, \underline{z})) \cdot c_{Tip}(t, \underline{z}), \quad \underline{z} \in R^3. \tag{6}$$

The apical growth rate is a function of a mean value of dL_1/dt, i.e. $\bar{\alpha}$, which is observed under ideal nutrient supply, and a function of the local growth activity $\psi_{Tip}(\underline{c}_S(t, \underline{z}))$. $\bar{\alpha}$ is usually smaller than α_m from Eq. (3) due to the assumption of constant elongation velocity. For ψ_{tip} Michaelis-Menten type kinetics can be used.

Colonies on solid agars and thin sections of pellets show a symmetric appearance. Therefore, a reduction to $\underline{z} \in R^1$ is possible. The radius of a pellet is then given by z_R.

To derive a balance equation for the local hyphal concentration a differential spherical shell is considered. Hyphae located in this shell do not leave it as they do not possess any means for motion due to the lack of subapical growth. However, they can be degraded, $r_{HyD}(t, z)$, or broken apart, $r_{HyB}(t, z)$:

$$\frac{\partial c_{Hy}(t, z)}{\partial t} = \bar{\alpha} \cdot \psi_{Tip}(\underline{c}_S(t, \underline{z})) \cdot c_{Tip}(t, \underline{z}) - r_{HyD}(t, z) - r_{HyB}(t, z). \tag{7}$$

The breakage rate is usually not only a function of the local conditions but of the history of the respective hypha as well [55].

3.1.2 *Tip Formation*

In microscopic investigations the hyphal growth unit, HGU, is a very well known value to characterise a mycelium. It represents the ratio of the total hyphal length to the number of tips. The HGU can be interpreted as the mean length available for every growth centre. In experiments and in the simulations shown above the HGU very soon becomes constant. Hence, if the total hyphal length grows, the number of tips has to grow accordingly, for example with

$$r_{Tip}(t, z) = \bar{\beta} \cdot \psi_{Hy}(\underline{c}_S(t, z)) \cdot c_{Hy}(t, z), \tag{8}$$

where $\bar{\beta}$, ψ_{Hy} and c_{Hy} are the mean branching rate, the activity of branching and the local concentration of hyphae, respectively.

In contrast to hyphae, tips do 'move' or are 'transported' due to apical growth. For a nondirectional growth this movement is proportional to the local gradient of hyphal elongation velocity, i.e. $\partial r_{Hy}/\partial z$, showing a diffusion-like behaviour. Again, degradation and breakage are considered, too. In radial coordinates the balance reads

$$\frac{\partial c_{Tip}(t, z)}{\partial t} = \frac{1}{z^2} \cdot \frac{\partial}{\partial z}\left(k_{Tip} \cdot \bar{\alpha} \cdot z^2 \cdot \frac{\partial(\psi_{Tip} \cdot c_{Tip})}{\partial z}\right)$$
$$+ \bar{\beta} \cdot \psi_{Hy}(\underline{c}_S(t, z)) \cdot c_{Hy}(t, z) - r_{TipD}(t, z) - r_{TipB}(t, z). \tag{9}$$

For all equations appropriate initial and boundary equations have to be formulated, e.g.

$$\left.\frac{\partial(\psi_{Tip} \cdot c_{Tip})}{\partial z}\right|_{z=0} = 0 \tag{10}$$

$$\left(k_{Tip} \cdot \bar{\alpha} \cdot \frac{\partial \psi_{Tip} \cdot c_{Tip})}{\partial z}\right)\Bigg|_{z=z_R} = \frac{dz_R(t)}{dt} \cdot c_{Tip}(t, z_R) \tag{11}$$

$$c_{Tip}(t_0, z) = c_{Tip0}(z). \tag{12}$$

In the boundary equation (11) it is assumed that tips moving over the pellet radius $z = z_R$ imply an increase in pellet radius. The importance of the formulation of a moving boundary problem should not be underestimated. There is no physical argument why only growth inside a pellet but not on the boundary should be considered. Hence, an assumption of nongrowing pellets, as mentioned above, cannot lead to meaningful results. This was confirmed during the development of the model when other definitions of the moving boundary led to different profiles of the concentrations of hyphae and tips. Therefore, a correct boundary formulation is crucial.

3.1.3
Pellet Radius

The change in pellet radius is defined by the motion of that tip which has the largest distance to the centre:

$$\frac{dz_R(t)}{dt} = \gamma \cdot \bar{\alpha} \cdot \psi_{Tip}(\varsigma_S(t, z_R)). \tag{13}$$

As hyphae do not grow straight ahead the factor γ has to be introduced, which is smaller than 1. It can be determined from microscopic experiments or from simulations with the microscopic model.

3.1.4
Substrates

The balance equations for the substrates inside a pellet can be easily derived:

$$\frac{\partial c_{Si}(t, z)}{\partial t} = \frac{1}{z^2} \cdot \frac{\partial}{\partial z}\left(D_{Si,eff} \cdot z^2 \cdot \frac{\partial c_{Si}(t, z)}{\partial z}\right) - r_{Si}(t, z), \quad i = 1, \ldots, M \tag{14}$$

$$\frac{\partial c_{Si}(t, z)}{\partial z}\Bigg|_{z=0} = 0, \quad i = 1, \ldots, M \tag{15}$$

$$D_{Si,eff} \cdot \frac{\partial c_{Si}(t, z)}{\partial}\Bigg|_{z=z_R} = k_{Si} \cdot (c_{SiL}(t) - c_{Si}(t, z_R)), \quad i = 1, \ldots, M \tag{16}$$

$$c_{Si}(t_0, z) = c_{Si0}(z), \quad i = 1, \ldots, M. \tag{17}$$

$D_{Si,eff}$, r_{Si} and c_{SiL} represent the effective diffusion coefficient of substrate i based on the void volume in a pellet, all substrate consuming reactions, and the

concentrations of the substrates in the bulk, respectively. Equations for the substrate concentrations in the bulk can be derived easily. For a detailed discussion of all assumptions included in this model see [53].

3.2 Simulation and Application Studies

Although the model is outlined for all substrates, only oxygen is considered here due to its low solubility. In most cases the other substrates give rise to an approximately uniform behaviour inside a pellet. This does not apply to continuous or to some fed-batch processes in which a depletion of other substrates inside a pellet can occur. However, these cases are not considered here for simplicity.

Figure 8 shows the simulated development [33] of the concentrations of hyphae, tips and oxygen of a growing pellet as a function of spatial location inside the pellet without degradation and breakage. The radii for different time instants can be best estimated from the span of the oxygen concentration profiles. Initial profiles c_{Hy0} and c_{Tip0} are taken from a simulation with the microscopic model. The oxygen concentration is assumed to be uniform over the pellet radius for t = 0. The simulation results show that after an initial increase in hyphal length and therefore biomass in the centre of the pellet (z = 0), growth is restricted to the outer part after some 10 h.

In [42, 53] it is shown that this model describes experimentally determined oxygen profiles very well.

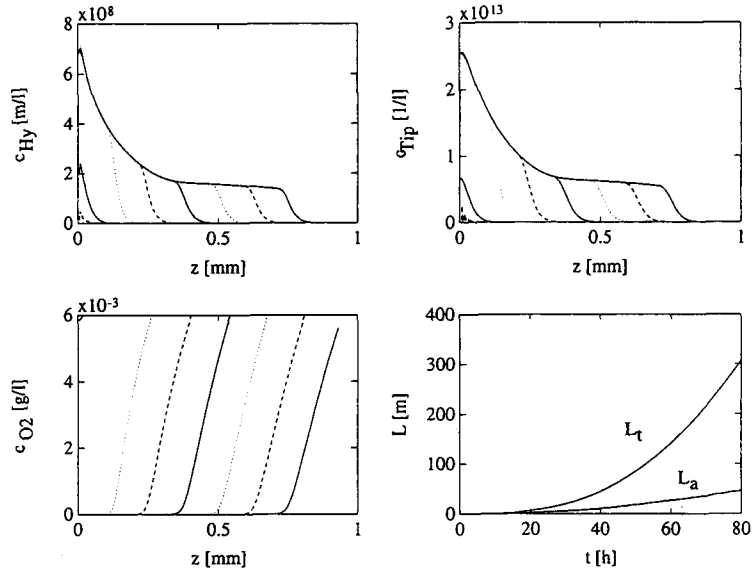

Fig. 8. Simulation of the concentrations of hyphae, tips and oxygen as a function of z for t = 0, 6, 18, 30, 42, 54, 66, 78 h and simulated development of the total hyphal length of a pellet, L_t, and of that part of a pellet which is supplied by oxygen, L_a (active length)

In the center of the pellet a growing zone without oxygen can be observed in which neither growth nor production takes place. As a result hyphae (and tips) are degraded, leaving a pellet with an empty core. This phenomenon can be included in the model by appropriate expressions for r_{HyD} and r_{TipD} (not done here). Instead, a simulation with the microscopic model [26] is given in Fig. 9, including an approximate approach for mass transport as well as degradation of hyphae some time after depletion of oxygen. The simulation results in Fig. 9 resemble quite well pictures known from microscopy.

Returning to Fig. 8, two additional variables are shown as functions of time: the total hyphal length (L_t) and that part of the total hyphal length which is supplied with oxygen, called active length here (L_a). These variables will be important in a model reduction explained below. They can be obtained by integration over the whole pellet and the active part of the pellet, respectively. It should be noted that the concentrations of hyphae and tips are formulated as length and number of tips per volume, respectively. The results in Fig. 8 show that an exponential growth at the beginning is followed by an increase which is approximately proportional to t^3. This behaviour is known as the 'cube root law' [45].

3.2.1 *Production*

To show an application of this model, the production of the antibiotic Nikkomycin by *Streptomyces tendae* is considered in a fluidized-bed reactor. In

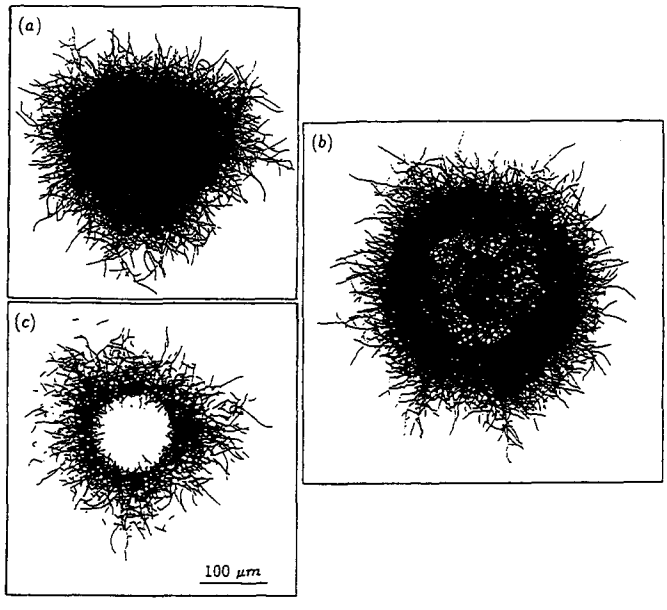

Fig. 9 a–c. Simulation with the microscopic model including oxygen transport into the pellet and degradation of hyphae, from Yang [26]: **a** 7 h; **b** 20 h; **c** simulated 2 µm thin section for t = 17 h

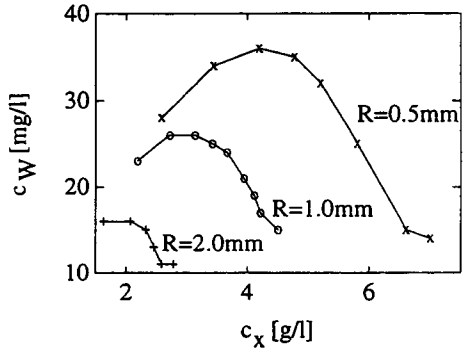

Fig. 10. Stationary concentration of Nikkomycin, c_w, as a function of biomass, c_x, determined during the growth phase, and of radius R of the carriers. The porosity amounts to 0.5

this application the organisms are grown on carriers, which are retained in the reactor. As a result, it is very easy to apply different optimal media for the growth and the production phase by a complete medium exchange [56]. However, the optimal values for the amount of biomass grown on the carriers, as well as the radius and the porosity of the carriers used, have to be determined in time consuming experiments. To get a first idea, the above stated model is extended to describe growth into and on a carrier. Figure 10 shows results of simulations in which the concentration of the antibiotic in the stationary production phase is determined as a function of radius and porosity of the carriers and of the concentration of biomass, c_x, grown on the carriers during the growth phase. For the production rate of Nikkomycin a very simple expression

$$r_W(t,z) = k_m \cdot \frac{c_{O_2}(t,z) - c^*_{O_2}}{c_{O_2}(t,z) + K_{O_2W}} \cdot c_{Hy}(t,z) \tag{18}$$

is used. Pronounced maxima can be observed for different sizes of the carriers. These results can now be used to minimize the amount of experiments needed to determine finally optimal production conditions.

3.3 Comparison of the Model with Other Approaches

3.3.1 *Microscopic Model*

For those regions of operation where both the microscopic and the pellet model are valid, identical results should be obtained. This is especially true when there is no limitation in oxygen supply; see Fig. 11. Here, the initial profiles c_{Hy0} and c_{Tip0} of the pellet model for $t = t_0 = 16$ h are taken from a simulation of the microscopic model. By adaptation of the diffusion parameter k_{Tip}, see Eq. (9), it

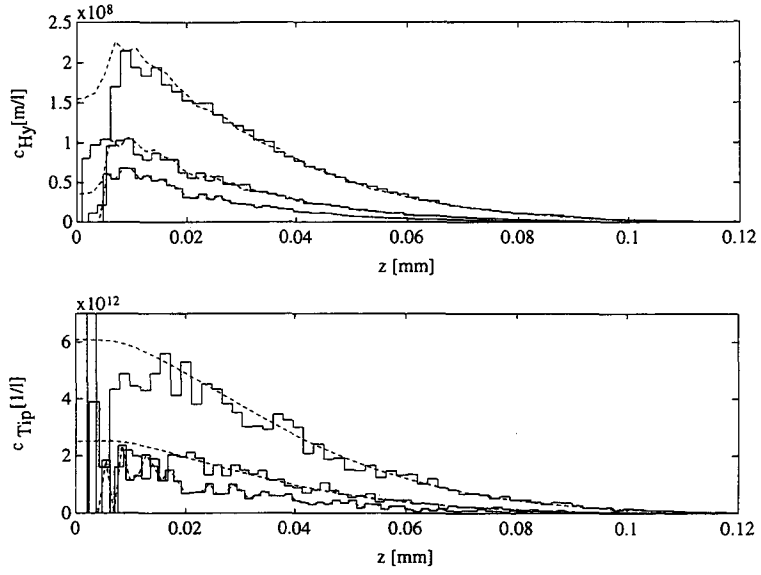

Fig. 11. Comparison of simulations obtained with the microscopic model (—) and pellet model (---) for t = 16 h, 17.6 and 20 h; from Buschulte [53]

is possible to predict the same development using the very different models (Fig. 11). Hence, it is shown that the consideration of local concentrations of hyphae and tips which is adopted in the pellet model leads to meaningful results.

3.3.2
Pellet Model Without Tips

Equations (6) and (8) are based on a model of Schuhmann and Bergter who describe growth of a small mycelium [57]. In this model the total hyphal length L_t increases proportionally to the number of tips N

$$\frac{dL_t(t)}{dt} = \bar{\alpha} \cdot N(t) \tag{19}$$

and the number of tips increases proportionally to the total hyphal length

$$\frac{dN(t)}{dt} = \bar{\beta} \cdot L_t(t). \tag{20}$$

With the initial conditions $L_t(0) = L_{t0}$ and $N(0) = 1$ integration yields

$$L_t(t) = \frac{1}{2}\left(\frac{\bar{\alpha}}{\bar{\mu}} + L_{t0}\right) \cdot e^{\bar{\mu} \cdot t} + \frac{1}{2}\left(L_{t0} - \frac{\bar{\alpha}}{\bar{\mu}}\right) \cdot e^{-\bar{\mu} \cdot t} \tag{21}$$

$$N(t) = \frac{1}{2}\left(\frac{L_{t0}}{HGU} + 1\right) \cdot e^{\bar{\mu} \cdot t} + \frac{1}{2}\left(1 - \frac{L_{t0}}{HGU}\right) \cdot e^{-\bar{\mu} \cdot t}, \tag{22}$$

with

$$HGU = \lim_{t \to \infty} \frac{L_t(t)}{N(t)} = \sqrt{\frac{\bar{\alpha}}{\bar{\beta}}} \tag{23}$$

and

$$\bar{\mu} = \sqrt{\bar{\alpha} \cdot \bar{\beta}}. \tag{24}$$

For $t \to \infty$ exponential growth follows:

$$\frac{dL_t(t)}{dt} \approx \bar{\mu} \cdot L_t(t). \tag{25}$$

This result is now used for a further reduction of the pellet model. If only the local concentration of hyphae is considered, a single equation can be given for the biotic phase in which a formal diffusion of hyphae is introduced:

$$\frac{\partial c_{Hy}(t,z)}{\partial t} = \frac{1}{z^2} \cdot \frac{\partial}{\partial z}\left(k_{Hy} \cdot \bar{\mu} \cdot z^2 \cdot \frac{\partial(\psi_{Hy} \cdot c_{Hy})}{\partial z}\right) + \bar{\mu} \cdot \psi_{Hy} \cdot c_{Hy} - r_{HyD}(t,z) - r_{HyB}(t,z). \tag{26}$$

The development of the total length L_t of hyphae calculated on this basis gives the same results as with the pellet model considered so far. A comparison of the results in Fig. 8 and Fig. 12 reveals, however minor differences in the concentration profiles as a function of radius.

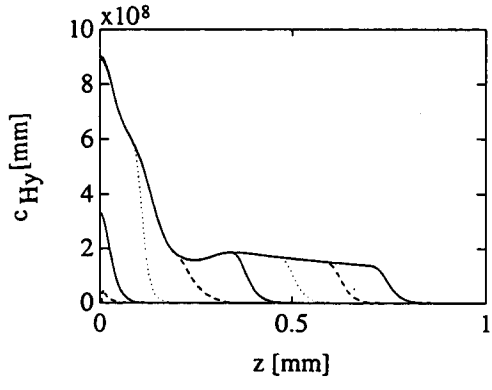

Fig. 12. Simulation of the local hyphal concentration as a function of the radius for t = 0, 6, 18, 30, 42, 54, 66, 78 h with model (26)

3.3.3
Lumped Pellet Model

A comparison of different simulations based on the original pellet model indicates that the development of total hyphal length, $L_t(t)$, and therefore biomass, can be explained by a much simpler lumped model. Such a model reduction is necessary when in the next step the behaviour of a population of pellets of different sizes has to be described mathematically. This also requires information about the active length $L_a(t)$, since this quantity determines maintenance demands. However, active length L_a is not a state variable in the sense of system theory. When a large pellet ($L_t > L_a$) is torn up into smaller pellets by the stirrer, all small pellets i might be perfectly supplied with oxygen ($L_{ti} = L_{ai}$). The amount of active biomass is therefore not conserved ($\Sigma L_{ai} \neq L_a$) as would be expected for a state variable. Hence, no differential equation should be used to describe L_a.

A simple black-box model for $L_t(t)$ is given here which is based on numerous simulation studies with the complete pellet model in which combinations of different values of $\bar{\alpha}$, $\bar{\beta}$ and c_{O_2L} are used to build up a data base for model identification.

As long as total hyphal length is less then a critical value, $L_t < L_{cr}$, the model reads

$$\frac{dL_t(t)}{dt} = a_1 \cdot \mu\,(c_{O_2L}(t)) \cdot L_t(t), \quad L_a(t) = \frac{1}{a_1 \cdot \bar{\mu}} \cdot \frac{dL_t(t)}{dt}, \tag{27}$$

with

$$\mu(c_{O_2L}(t)) = \bar{\mu} \cdot \frac{c_{O_2L}(t)}{c_{O_2L}(t) + K_{O_2L}}, \quad \bar{\mu} = \sqrt{\bar{\alpha} \cdot \bar{\beta}}. \tag{28}$$

For growing pellet sizes ($L_t(t) > L_{cr}$) growth rate decreases according to Eq. (29) from exponential behaviour to smaller values:

$$\frac{dL_t(t)}{dt} = \frac{1 + a_2 \cdot \bar{\beta} \cdot L_{cr}^{\lambda}}{1 + a_2 \cdot \bar{\beta} \cdot L_t^{\lambda}(t)} \cdot a_1 \cdot \mu(c_{O_2L}(t)) \cdot L_t(t) \tag{29}$$

$$L_a(t) = \frac{a_6 \cdot L_t(t)}{1 + a_4 \cdot \bar{\mu}^{-a_5} \cdot L_t x(t)} \cdot \frac{dL_t(t)}{dt}, \quad a_6 = \frac{1 + a_4 \cdot \bar{\mu}^{-a_5} \cdot L_{cr}}{a_1 \cdot \bar{\mu} \cdot L_{cr}}. \tag{30}$$

One set of constant parameters a_i, l_{cr}, λ and K_{O_2L} is identified from the above-mentioned simulations with the complete pellet model (see Table 1).

Figure 13 shows a comparison of the complete and the reduced model. In both cases the oxygen concentration of the bulk, c_{O_2L}, is calculated according to an appropriate balance equation. There is excellent agreement between the complete and the reduced model, indicating that the latter can be used from a macroscopic point of view to describe pellet growth in a population balance.

Table 1. Parameters of the lumped model

L_{cr}	a_1	a_2	a_3	a_4	a_5	λ	K_{O_2L}
0.132 m	1.37	233 $\mu m^{0.622}$ h	$0.7 \frac{1}{\mu m^{0.622}}$	$2.53 \frac{h^{0.51}}{\mu m}$	0.51	0.378	$0.0797 \frac{g}{l}$

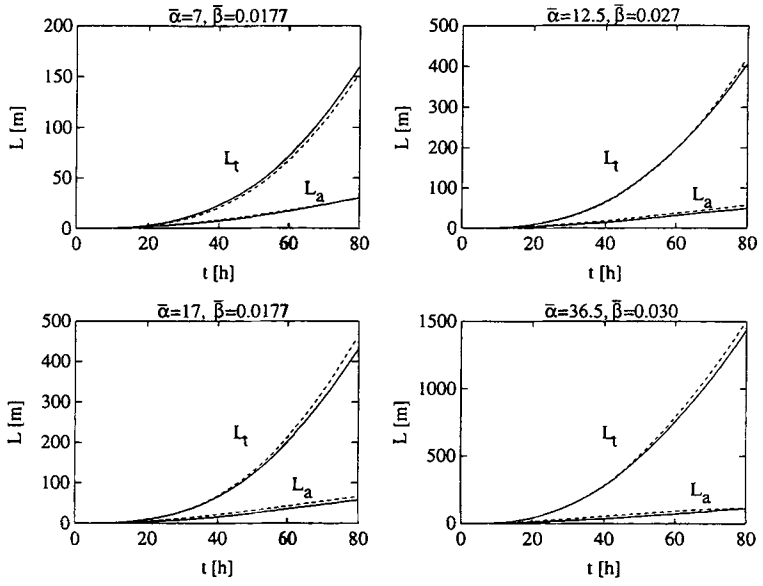

Fig. 13. Comparison of total hyphal length L_t and active hyphal length L_a for different values of $\bar{\alpha}$ ([μm/h]) and $\bar{\beta}$ ([1/(μm · h)]). Complete model (——), reduced model (– – –)

For c_{O_2L} = const. and $t \to \infty$ Eq. (29) yields

$$\frac{dL_t(t)}{dt} \approx d_1 \cdot L_t^{1-\lambda}(t) \Rightarrow L_t(t) \approx d_1' \cdot t^{1/\lambda} + d_2. \tag{31}$$

In the identification the exponent $1/\lambda$ according to Eq. (31) is found to be 2.65. A similar result has already been named as the cube root law [45].

4 Morphology in a Submerged Culture

Simulations with the pellet model show that even single pellets are not uniformly supplied with substrates. In cultivations this inhomogeneity is superposed by a pronounced pellet size distribution. Apart from its direct influence

on growth and production behaviour in batch, fed-batch or continuous processes this pellet size distribution is of major interest in terms of rheology, heat and mass transfer, e.g. in the context of correlations between these variables. To tackle such kinds of questions a fundamental understanding and a quantitative description of the processes going on in a pellet containing cultivation are necessary. Both experimental and theoretical tools are available today. On one hand image analysis provides an ideal experimental set-up to gain primary data, cf. [58] or Thomas in this volume. Fully automated versions including sampling, sample preparation, image analysis and wash cycles are available [4]. On the other hand, segregated models, especially population balances, are known to describe the influences of processes such as particle birth, growth, breakage and agglomeration on pellet size distribution. In the following section some approaches are summarized.

4.1 Population Balances

Pellet size distribution can be described by a number density function $f(\underline{y}, t)$, in which $\underline{y}$ are characteristic properties, such as total hyphal length, mass of a pellet, age, etc. Only a few attempts have been made so far to describe the development of the pellet size distribution in mycelial cultivations. Nielsen [12] introduces pellet mass and number of tips as characteristic properties; see also Krabben and Nielsen in this volume. After some assumptions they reduce the problem to two ordinary differential equations describing average values. The special influences of mass transport processes inside a pellet on its behaviour are not taken into account as only small mycelia are considered. Mass transport is also not included in Edelstein [59] and Tough [60].

The lumped pellet model discussed above, however, includes these most important effects. Therefore, total hyphal length L_t can be used as a characteristic property, when Eqs. (27–30) are used to account for the influence of oxygen.

As L_t increases exponentially the following population balance is formulated with a normalized characteristic property, i.e. $s = \ln(L_t/L_0)$. L_0 is the length of a spore. To derive the population balance a term $(V(t) \cdot f(s, t) \cdot ds)$ is considered for small values of ds. It represents the number of pellets with a total hyphal length between s and s + ds at time t in volume V(t). This number changes because of pellets growing into and out of the segments [s, s + ds), pellets being washed out of the fermenter and pellets appearing or disappearing due to processes such as

- $\sigma_1(s, t, \ldots)$ birth,
- $\sigma_2(s, t, \ldots)$ death,
- $\sigma_3(s, t, \ldots)$ breakage or
- $\sigma_4(s, t, \ldots)$ agglomeration.

A balance over the number of pellets in a segment [s, s + ds) with ds → 0 yields

$$\frac{\partial}{\partial t}\left[V(t)\cdot f(s,t)\right] = -V(t)\cdot\frac{\partial}{\partial s}\left[u(s,t,\ldots)\cdot f(s,t)\right] + Q_i(t)\cdot f_i(s,t) - Q_o(t)\cdot f(s,t) + V(t)\cdot\sum_{j=1}^{4}\sigma_j(s,t,\ldots),$$

$$t \geq t_0, \qquad s \geq s_0, \tag{32}$$

in which u and $Q_{i,o}$ are the growth velocity of a single pellet and the volumetric flows into and out of the system, respectively. As some σ_j are expressed by integrals the resulting equation is of a non-linear integro-partial differential type. For $Q_i = Q_o = Q, q = Q/V, V = \text{const.}, f_i = 0$, neglecting death and agglomeration processes and introducing a rate of breakage $r_3 = k_z \cdot \exp(\eta \cdot s) \cdot f(s,t)$, the population balance reads [33]

$$\frac{\partial f(s,t)}{\partial t} = -a_1\cdot\mu(c_{O_2}(t))\cdot\frac{\partial}{\partial s}\left[\hat{u}\cdot f(s,t)\right] - q(t)\cdot f(s,t) - k_z\cdot e^{\eta\cdot s}\cdot f(s,t) + \int_{\ln(e^s+1)}^{\infty} 2\cdot p(s',s,t)\cdot k_z\cdot e^{\eta\cdot s}\cdot f(s',t)\,ds', \tag{33}$$

with

$$\hat{u} = \begin{cases} 1 & \text{for} \quad s \leq s_{cr} \\ \dfrac{1+d_3\cdot e^{\lambda\cdot s_{cr}}}{1+d_3\cdot e^{\lambda\cdot s(t)}} & \text{for} \quad s > s_{cr} \end{cases}. \tag{34}$$

The birth process, σ_1, indicating germination, is included in the boundary condition. The germination rate $r_G(c_{Sp}, \underline{c}_S, t)$ is assumed to be a function of the spore concentration $c_{Sp}(t)$ and the substrate concentration $\underline{c}_S(t)$:

$$\sigma_1(s,t,c_{Sp},\underline{c}_S) = r_G(c_{Sp},\underline{c}_S,t)\cdot f_G(s,t). \tag{35}$$

The number density function $f_G(s,t)$ of particles produced by birth is usually known. In the example shown here all particles produced by birth have the same size, i.e. $s^* = s_0 = \ln(1) = 0$. Hence, the smallest particle considered is a spore which just has started germination. The number density function $f_G(s,t)$ of new particles then reduces to a Dirac pulse:

$$f_G(s,t) = \delta(s - s_0). \tag{36}$$

If $f(s,t)$, $\partial f(s,t)/\partial s$ and $f_i(s,t)$ are bounded for $s \to s_0$ a balance of the element $[s_0, s_0 + ds)$ with ds → 0 yields the missing boundary condition

$$a_1\cdot\mu(c_{O_2L}(t))\cdot f(s,t)\,|_{\,s=s_0} = r_G(c_{Sp},\underline{c}_S,t). \tag{37}$$

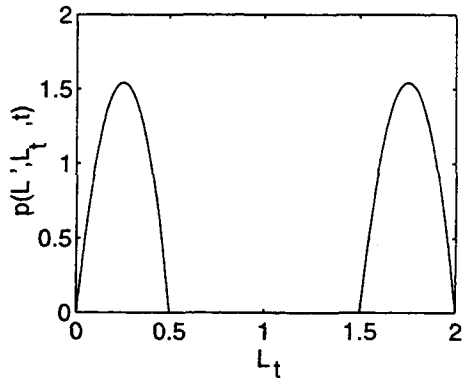

Fig. 14. Density of the breakage probability as a function of L_t

For the germination rate, r_G, a first order rate equation is assumed. The balance for the ungerminated spores reads

$$\frac{dc_{Sp}(t)}{dt} = -r_G(t) - q \cdot c_{Sp}(t)$$
$$= -k_G \cdot c_{Sp}(t) - q \cdot c_{Sp}(t). \tag{38}$$

An example of the breakage probability $p(s', s, t)$ in terms of the original variable L_t is shown in Fig. 14. This kind of presentation is chosen since the symmetry of p is lost upon transformation with $s = \ln(L_t/L_0)$.

All pellets consume oxygen for growth, which is proportional to ds/dt, and for maintenance. The latter is proportional to the amount of active hyphal length $L_a = L_0 \cdot \exp(s_a)$. A balance yields

$$\frac{dc_{O_2L}(t)}{dt} = q(t) \cdot (c_{O_2in}(t) - c_{O_2L}(t)) + k_La \cdot (c^*_{O_2} - c_{O_2L}(t))$$
$$- L_0 \cdot \int_0^\infty (Y_{O_2g} \cdot e^{s(t)} \cdot \frac{ds(t)}{dt}\Big|_{Pellet} + Y_{O_2m} \cdot e^{s_a(t)}) \cdot f(s,t)\, ds \cdot \tag{39}$$

In Eq. (39) no additional account for mass transfer inside a pellet has to be included, as this behaviour is already part of the reduced pellet model.

4.2 Simulation and Qualitative Comparison with Experimental Results

After a discretization of s, and evaluation of the integrals by trapezoidal rule, a numerical solution of the coupled equation is obtained. Figure 15 shows the result of a simulation. At the beginning, the pellet size distribution moves

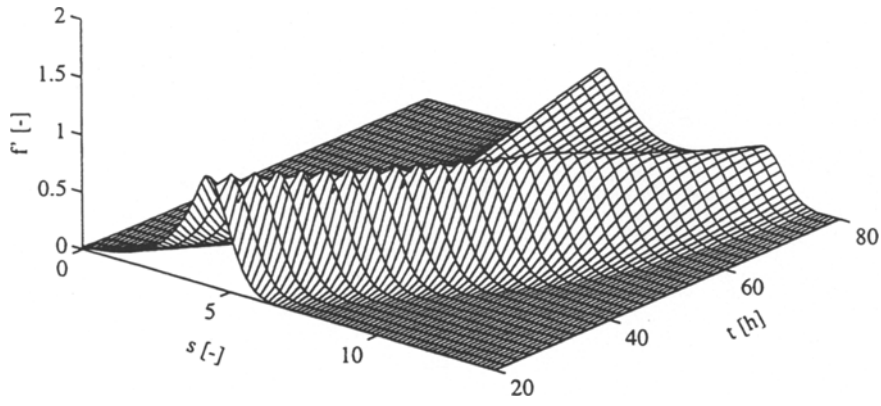

Fig. 15. Development of the normalised number density function $f' = f/f_0$ [61]

towards larger values of s. With growing sizes more and more pellets are broken down into smaller parts. A new subpopulation of smaller pellets emerges.

Figure 16 shows another simulation in which a parameter of the breakage probability is varied. Here, s_{II} relates to a length L_{II} for which the breakage probability becomes zero for the first time (0.5 in Fig. 14).

From the number density function more information can be gained. By integration the total number of pellets

$$F(t) = \int_{s_0}^{\infty} f(s,t)\, ds \tag{40}$$

or total amount of biomass

$$m_t = \sigma_{Hy} \cdot L_0 \cdot \int_{s_0}^{\infty} e^s \cdot f(s,t)\, ds \tag{41}$$

can be obtained.

A very first approach of adapting the model to experimental conditions shows that the behaviour determined in experiments by image analysis [58] can already be described qualitatively (see Fig. 17). When comparing the results it should be noted that in the simulation a distribution is calculated as a continuous function of the normalized hyphal length while the experimental data are given for discrete size classes given as pellet area. To allow at least a rough comparison a relation has to be found between the total hyphal length of a pellet and the pellet area. Therefore, Eqs. (27, and 29) are transformed to the new coordinate s, i.e. ds/dt. Then, Eq. (13)

$$\frac{dz_R(t)}{dt} = \gamma \cdot \bar{\alpha} \cdot \frac{c_{O_2}}{K_{O_2} + c_{O_2}}$$

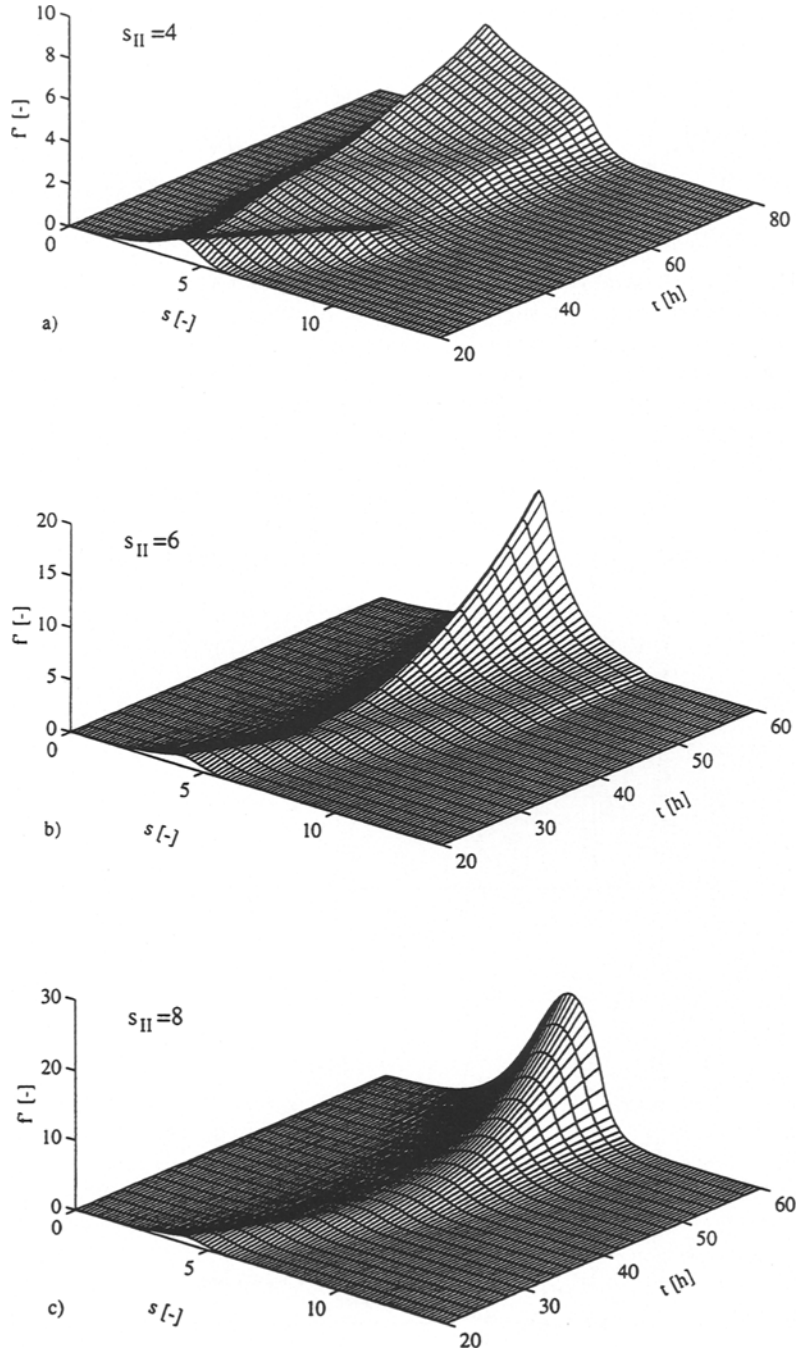

Fig. 16. Development of the normalised number density function $f' = f/f_0$ for different values of s_{II}; see text

is divided by the transformed Eqs. (27, and 29) to give

$$\frac{dz_R(t)}{ds} = \begin{cases} \dfrac{\gamma \cdot \bar{\alpha}}{a_1 \cdot \mu} & \text{for } s(t) \le s_{cr} \\ \dfrac{\gamma \cdot \bar{\alpha} \cdot (1 + d_3 \cdot \lambda^{\cdot s(t)})}{a_1 \cdot \bar{\mu} \cdot (1 + d_3 \cdot e^{\lambda \cdot s_{cr}})} & \text{for } s(t) > s_{cr} \end{cases}$$

These equations can easily be integrated to relate the radius z_R and therefore the pellet area to the length s (see Fig. 17).

These first examples show that by means of population balances the influences of different factors on pellet size distributions can be studied. Based on such information further questions, e.g. concerning correlations with rheological parameters, can be addressed. However, before this can be done, more experimental data on breakage and agglomeration processes are needed. The methods provided by image analysis will be very helpful in this respect.

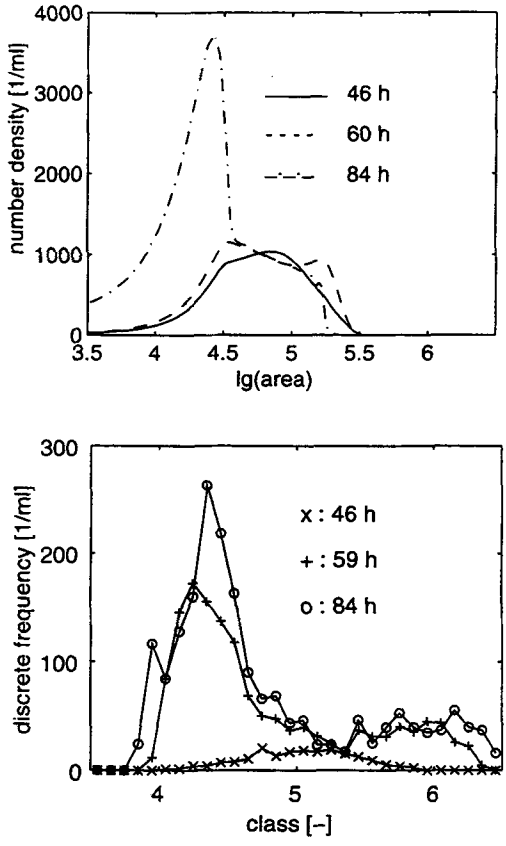

Fig. 17. Qualitative comparison of simulated pellet size distribution with experiments

5 References

1. Bushell ME (1988) Growth, product formation and fermentation technology. In: Goodfellow M, Williams ST, Mordanski M (eds) Actinomycetes in biotechnology. Academic Press, London, p 186
2. Fisher SH (1988) Nitrogen assimilation in streptomycetes. In: Okami Y, Beppu T, Ogawara H (eds) Biology of *Actinomycetes*. Japan Scientific Societies Press, Tokyo, p 47
3. Hirsch CF, McCann-McCormick PA (1985) Biology of streptomyces. In: Demain AL, Solomon NA (eds), Biology of industrial microorganisms. Benjamin/Cummings, Menlo Park, CA, p 291
4. Treskatis SK, Orgeldinger V, Wolf H, Gilles ED (1997) Biotechnol Bioeng 53:191
5. King R (1996) J Biotechnol 52:219
6. King R, Büdenbender Ch (1996) J Biotechnol 52:235
7. Bergter F (1978) Z Allg Mikrobiol 2:143
8. Cagney JW, Chittur VK, Lim HC (1984) Biotechnol Bioeng Symp 14:619
9. Megee RD III, Kinoshita S, Fredrickson AG, Tsuchiya HM (1970) Biotechnol Bioeng 12:771
10. Matsumura M, Imanaka T, Yoshida T, Taguchi H (1981) J Ferment Tech (Japan) 59:115
11. Nestaas E, Wang DIC (1983) Biotechnol Bioeng 25:781
12. Nielsen J (1992) Modelling the growth of filamentous fungi. In: Fiechter A (ed) Adv Biochem Eng Biotechnol 46, Springer, Berlin Heidelberg New York, p 187
13. Patankar DB, Liu TC, Oolman T (1993) Biotechnol Bioeng 42:571
14. Paul GC, Thomas CR (1996) Biotechnol Bioeng 51:558
15. Aynsley M, Ward AC, Wright AR (1990) Biotechnol Bioeng 35:820
16. Prosser JI, Trinci APJ (1979) J of Gen Microbiol 111:153
17. Lejeune R, Baron GV Accepted for Biotechnol Bioeng
18. King R, Buschulte TK, Yang H, Gilles ED (1990) Mathematical models of filamentously growing microorganisms. In: Behrens D (ed) Dechema Biotechnology Conferences, vol. 4. Verlag Chemie, Frankfurt, p 989
19. Yang H (1994) Mathematische Modellierung des Wachstums myzelbildender Mikroorganismen. PhD thesis, Universität Stuttgart
20. Yang H, King R, Reichl U, Gilles ED (1992) Biotechnol Bioeng 39:49
21. Yang H, Reichl U, King R, Gilles ED (1992) Biotechnol Bioeng 39:44
22. Shomura T, Yoshida J, Amano S, Kojima M, Inouye S, Niida T 81979) J Antibiotics 32:427
23. Vitális S, Szabó G, Vályi-Nagy T (1963) Acta Biol Hung 14:1
24. Reichl U, King R, Gilles ED (1991) Biotechnol Bioeng 32:193
25. Prosser JI, Tough AJ (1991) Crit Rev Biotechnol 10:253
26. Yang H (1993) Mathematical model for filamentous growth of mycelial microorganisms in lab chamber and in batch, fed-batch and continuous cultures. In: Alberghina (ed) ECB 6. Elsevier, Amsterdam, p 845
27. Meyerhoff J, Tiller V, Bellgardt KH (1995) Bioproc Eng 12: 305
28. Kummer C, Kretschmer S (1986) J Basic Microbiol 26:27
29. Prosser JI, Gray DI, Gooday GW (1988) Cellular mechanisms for growth and branch formation in streptomycetes. In: Okami Y, Beppu T, Ogawara H (eds) Biology of actinomycetes. Japan Scientific Societies Press, Tokyo, p 316
30. Riesenberg D, Bergter F (1979) Z Allg Mikrobiol 19:415
31. Treskatis S, Reichl U, Orgeldinger V, King R, Gilles ED (1992) Process control of fermentations with filamentous microorganisms by means of digital image processing and pattern recognition. Poster, 6th Europ Conf on Biotechnology, Florence, Italy
32. Reichl U, Yang H, Gilles ED, Wolf H (1990) FEMS Microbiol Letters 67:207
33. King R (1994) Mathematische Modelle myzelförmig wachsender Mikroorganismen. Fortschrittsber 17, 103, VDI, Düsseldorf
34. Reichl U (1991) Einsatz eines Bildverarbeitungssystems zur Erfassung der Morphologie und des Wachstums mzyelbildender Mikroorganismen in submerser Kultur. PhD thesis, Universität Stuttgart

35. Reichl U, Buschulte TK, Gilles ED (1990) J Micros 158:55
36. Kretschmer S (1989) J Basic Microbiol 29:587
37. Fiddy C, Trinci APJ (1976) J Gen Microbiol 97:167
38. Gray DI, Gooday GW, Prosser JI (1990) J Microbiol Meth 12:163
39. Neidhardt FC, Ingraham JL, Schaechter M (1990) Physiology of the bacterial cell: a molecular approach. Sinauer Associates, Sunderland, MA
40. Braun S, Vecht-Lifshitz SE (1991) TIBTECH 9:63
41. Wittler R, Baumgart H, Lübbers DW, Schügerl K (1986) Biotechnol Bioeng 28:1024
42. Buschulte TK, Yang H, King R, Gilles ED (1991) Formation and growth of pellets of streptomyces. In: Reuß M, Chmiel H, Gilles ED, Knackmus HJ (eds) Biochemical Engineering – Stuttgart. G. Fischer, Stuttgart, p 393
43. Chiu ZS, Zajic JE (1976) Biotechnol Bioeng 18:1167
44. Koch AL (1975) J Gen Microbiol 89:209
45. Emerson S (1950) J Bacteriol 60:221
46. Aiba S, Kobayashi K (1971) Biotechnol Bioeng 13:583
47. Kobayashi T, van Dedem G, Moo-Young M (1973) Biotechnol Bioeng 15:27
48. Phillips DH (1966) Biotechnol Bioeng 8:456
49. Pirt SJ (1966) Proc Roy Soc London B166:369
50. Yano T, Kodama T, Yamada K (1961) Agr Biol Chem 25:580
51. Chang HN, Moo-Young M (1988) Appl Microbiol Biotechnol 29:107
52. Skowlund CT (1990) Biotechnol Bioeng 35:502
53. Buschulte TK (1992) Mathematische Modellbildung und Simulation von Zellwachstum, Stofftransport und Stoffwechsel in Pellets aus *Streptomyceten*. PhD thesis, Universität Stuttgart
54. Buschulte TK, Gilles ED (1990) Modeling and simulation of hyphal growth, metabolism and mass transfer in pellets of streptomyces. In: Christiansen C, Munck L, Villadsen J (eds) Proceedings of the 5th European Congress on Biotechnology, p 279
55. Taguchi H (1971) The nature of fermentation fluids. In: Ghose TK, Fiechter A (eds) Advances in biochemical engineering 1. Springer, Berlin Heidelberg New York, p 1
56. Trück HU, Chmiel H, Hammes WP, Trösch W (1990) Appl Microbiol Biotechnol 33:139
57. Schuhmann E, Bergter F (1976) Z Allg Mikrobiol 16:201
58. Reichl U, King R, Gilles ED (1992) Biotechnol Bioeng 39:164
59. Edelstein L (1983) J Theor Biol 150:427
60. Tough AJ (1989) A theoretical model of *Streptomycete* growth in submerged culture. PhD thesis, University of Aberdeen
61. King R, Büdenbender Ch, Oswald G (1995) Mathematical models for growth and production of single pellets and pellet populations. In: Munack A, Schügerl K (eds) 6th Int Conf Computer Applications in Biotechnology. Dechema, Frankfurt, p 154

Received December 1996